

Chapter 3

SCALE EFFECTS AND THE MOLECULAR ORIGINS OF TRIBOLOGICAL BEHAVIOR

Gang He and Mark O. Robbins
Department of Physics and Astronomy
Johns Hopkins University
Baltimore, MD 21218
mr@pha.jhu.edu

1 INTRODUCTION

There has been a great deal of progress in probing the molecular origins of friction in recent years. New experimental tools such as the surface force apparatus,¹⁻³ quartz microbalance,⁴ scanning probe microscopy,⁵⁻⁶ and other methods,⁷⁻⁹ allow measurements with controlled chemistry and, in some cases, geometry. At the same time, tremendous increases in computer power have allowed increasingly sophisticated models of these ideal systems.¹⁰⁻¹¹

These nanotribological studies reveal behavior that can often be quite different than that observed at macroscopic scales. For example, crystalline monolayers exhibit no static friction on incommensurate substrates, and may even slide more easily than the fluid phase of the same monolayer!^{4,12} In contrast, most lubricants begin to exhibit solid-like behavior when confined in nanoscale contacts.^{1,3,10,13-15} Such dramatic changes with contact size have tremendous implications for the developing area of nanotechnology. They also pose questions of great fundamental interest about the molecular origins of conventional macroscopic behavior.

In the following sections we outline some of our group's work on nanoscale contacts. We begin by describing work that examines the limits of continuum approaches, culminating in a discussion of confinement induced glass transitions. Then the static and kinetic friction of glassy films are explored and shown to provide a molecular-scale explanation for Amontons' laws.

2 COMPUTATIONAL METHODOLOGY

Our focus has been on exploring general phenomena using molecular dynamics (MD) simulations with relatively simple interaction potentials.

These allow us to quickly span a wide range of shear rates, system sizes, geometries and interactions. They also allow treatment of longer time and length scales than more detailed potentials.

In all of the work described below, the two sliding solids contain discrete atoms. To minimize the number of atoms, the elastic interactions within the solids are treated in an Einstein model. Each atom is coupled to its equilibrium position by a spring of stiffness κ . These equilibrium positions can form a crystalline or disordered surface. The coordinate system is chosen so that the surfaces lie in the x - y plane and are normal to the z -axis.

One important variable is the relative registry and orientation of the two surfaces. Identical, aligned crystals can easily lock together to produce static friction, while analytic studies indicate that incommensurate surfaces (those with no common periodicity) should slide with zero static friction.^{10,12,16-18} Our simulations use periodic boundary conditions in the plane of the surfaces, and so can never be strictly incommensurate. However, we find that surfaces behave as if they were incommensurate once the common period becomes longer than a few lattice constants.¹⁸

In most of our simulations, a layer of “fluid” molecules is placed between the two solid surfaces. Some work considers spherical molecules that interact with a truncated Lennard-Jones potential:¹⁹

$$V_{LJ}(r) = 4\varepsilon\left[(\sigma/r)^{12} - (\sigma/r)^6\right], \quad r < r_c, \quad (1)$$

where r is the distance between molecules and the potential is zero for $r > r_c$. The parameters ε and σ are characteristic energy and length scales, respectively. The characteristic time is $t_{LJ} \equiv (\sigma^2 / m\varepsilon)^{1/2}$ where m is the molecular mass. These characteristic scales are used to normalize other quantities. Values that would be representative of hydrocarbons are²⁰ $\varepsilon \sim 30$ meV, $\sigma \sim 0.5$ nm and $t_{LJ} \sim 3$ ps.

Other simulations use a simple bead-spring model for oligomers.²⁰ Each molecule contains n spherical molecules of mass m . All monomers interact through a truncated Lennard-Jones potential, and adjacent monomers along the chain are coupled by an additional potential that prevents chains from crossing:

$$V_{CH}(r) = -(1/2)kR_0^2 \ln\left[1 - (r/R_0)^2\right], \quad (2)$$

where $R_0 = 1.5\sigma$ and $k = 30\varepsilon/\sigma^2$. Previous studies have shown that this bead-spring potential yields realistic dynamics for polymer melts,²⁰ and shown how to map between it and detailed chemical models of polymers.²¹ These detailed models take orders of magnitude more computer time than the bead-spring model.

Wall atoms interact with fluid molecules or monomers through a Lennard-Jones potential with modified parameters ε_w and σ_w . This allows us

to increase or decrease the amount of adhesion and the effective surface corrugation of the walls.

All of our runs are done in a constant temperature ensemble. In most cases a Langevin heat bath is coupled to the equations of motion of wall atoms.¹⁴ In the case of infinitely rigid walls $\kappa \rightarrow \infty$ the thermostat is instead coupled to the velocity components of the fluid molecules that are orthogonal to any imposed shear. We have performed extensive tests on the effects of thermostats.²² At the shear rates discussed below, their only effect is to prevent a gradual rise in temperature due to energy dissipated by friction. At higher shear rates, the structure and other properties of the film may be affected.²³⁻²⁴

It is well known that experimental measurements of friction are influenced by the mechanical properties of the measuring device. The same is true in simulations, and we have attempted to mimic typical surface force apparatus or atomic-force microscope experiments. For example, we generally apply a constant normal pressure, and allow the separation between surfaces to equilibrate.¹⁴ We find that using fixed wall separation can lead to very different behavior, especially when the walls are commensurate. The bottom wall is held fixed and the top wall is moved laterally by applying a constant velocity, a constant force, or by coupling the wall to a constant velocity stage with a spring. In most simulations the walls are also allowed to move freely in the direction normal to z and to the applied shear.

3 BREAKDOWN OF CONTINUUM BEHAVIOR AT NANOSCALES

A large number of studies have addressed the breakdown of continuum equations as lengthscales approach atomic dimensions.¹⁰ In the following we will focus on examples that our group has been involved in. The surprising conclusion is that continuum descriptions of elasticity and surface tension describe stresses down to a few lattice constants. Continuum viscoelastic equations can also apply to this scale. However, confinement in such small pores may change the phase of a fluid film, so that the appropriate value for the viscosity may differ dramatically from the bulk value.

3.1 Elasticity

Most analyses of the stress distribution near a contact are based on continuum elasticity. One might wonder whether such analyses are relevant in nanoscale contacts. Landman and coworkers²⁵ have examined this issue

for tips with a diameter of about 10 atoms and find a strong qualitative correspondence between the observed stresses and continuum calculations. However, one aspect of continuum calculations that cannot be correct is the prediction of infinite stresses at the edge of a contact. Such singularities are predicted by continuum theory whenever materials of sufficiently dissimilar elastic constants intersect at a sharp corner.²⁶ These mathematical singularities are unphysical and must be cut off in some manner at the atomic scale. The nature of this cutoff is important in determining the ultimate shear strength of a contact.

Vafek and Robbins have performed a detailed atomistic study of the stress near such corners.²⁷ At distances greater than a few lattice constants from the corner, the MD results agree quantitatively with continuum theory. When a perfectly harmonic interaction potential is used between the atoms, the singular behavior is cut off by the atomic size. For Lennard-Jones potentials, large stresses lead to anharmonic behavior within a few lattice constants from the corner, and eventually to plastic flow. One of the most intriguing results is that the maximum stress at the corner increases with system size. This can be understood from scaling analysis of the continuum equations.²⁶⁻²⁷

The observation that the peak stress at the edge of a contact decreases with contact diameter has potential consequences for nanodevices. In some models the large stresses at the edges of contacts facilitate sliding by nucleating defects.²⁸ If the stresses decrease in magnitude with the size of the contacts, the mechanism of sliding may change.

3.2 Surface Tension

As length scales decrease, capillary forces become increasingly important. Capillary forces are a major component of the normal load in many AFM and SFA experiments. Their magnitude is usually calculated with continuum theory and bulk surface tensions even though the radii of curvature of the meniscii may be only a few nanometers or less.

Thompson *et al.*²⁹ have calculated the Laplace pressure and contact angle of meniscii with radii of curvature as small as a few molecular diameters. They found that the results were in excellent agreement with continuum equations for all systems considered. Earlier work showed that even the non-equilibrium dynamic contact angle in systems of similar size could be described by continuum theory.³⁰

Figure 1 replots some of Thompson *et al.*'s data. Continuum theory predicts that the surface tension γ divided by the pressure drop across the interface ΔP should equal the radius of curvature ρ . As illustrated in the figure, values of $\gamma/\Delta P$ are consistent with directly measured radii of

curvature down to about 7 times a typical atomic diameter. It would be interesting to test this relation to even smaller radii in future work.

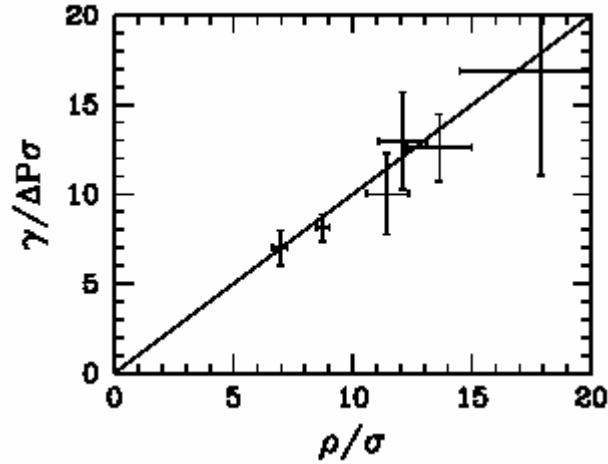


Figure 1. The radius of curvature ρ calculated from the pressure drop ΔP using the continuum relation $\rho = \gamma/\Delta P$ is plotted against the value of ρ measured directly from the meniscus geometry. The points should lie on the solid line if continuum theory applies.

3.3 Flow Boundary Conditions

Continuum theories of lubrication need boundary conditions to describe the dynamics at solid surfaces. The usual assumption is that there is no slip, i.e. that the two phases have the same velocity at the interface. However, a number of theoretical and experimental studies have shown that deviations from the no-slip boundary condition are common. They can be characterized by a slip length S that is normally of atomic dimensions,³¹⁻³² but can be much larger.³²⁻³⁵ Typical examples of slip for simple spherical molecules are shown in Fig. 2(b).

Calculations based on the no-slip assumption become inadequate when S is of the same order as the geometrical separation h between two interfaces. There are many cases where S is comparable to the minimum separation between lubricated surfaces in conventional applications. More dramatic effects can be expected at the ever shrinking average separations between hard disks and read heads, between the components of microelectromechanical machines, or in the tiny pipes being constructed with lithography.

3.4 Viscosity and Phase Changes

Many recent experimental^{1-3,13,36,37} and theoretical^{14,38-40} studies have examined the effect of confining walls on the viscosity of fluid films. Most fluids show bulk behavior when the separation h between the walls is more than ten molecular diameters. In this limit, their lubricating properties could be described by continuum equations with an appropriate flow boundary condition.

As the film thickness drops below a few to ten molecular diameters, the viscosity of most fluids diverges. Sharp divergences that are indicative of a first order phase transition are seen in some systems.^{13,14,38,39} Most systems exhibit a continuous divergence in the viscosity that is reminiscent of a bulk glass transition,^{2,14,38,39} but at temperatures and pressures that are far from the glass region in the bulk phase diagram. In fact, the molecules may not readily form glasses in the bulk, and the nature of this fluid/solid transition has been of considerable interest.

The onset of solid-like behavior in confined films has important implications for nanodevices and for boundary lubrication, where the separation between asperities on opposing surfaces decreases to molecular scales.⁴¹ For example, confinement-induced solidification would prevent lubricant from being squeezed out of contacts between static or moving surfaces. The remaining film would be able to accommodate shear, and thus help to lower both friction and wear.

3.4.1 Structural Changes

Even before films solidify there are dramatic changes in their structure. The most widely studied is ordering of atoms into layers that are parallel to the wall. This layering is induced by the sharp cutoff in fluid density at the wall and the bulk pair correlation function.⁴²⁻⁴⁴ A fluid layer forms at the preferred wall-fluid spacing. Additional fluid molecules then tend to lie in a second layer at the preferred fluid-fluid spacing, and so on.

Figure 2(a) illustrates layering of simple spherical molecules. The magnitude of the first peak depends strongly on the interaction between wall and fluid atoms ϵ_w , while the rate of decay of peaks into the fluid does not. This decay rate is determined by the decay of oscillations in the pair correlation function of the pure fluid.

Walls also induce epitaxial in-plane order in the fluid.^{32,45-47} This lateral registry is crucial to the transfer of shear stress and is inversely related to the amount of slip at the interface.³² It is illustrated in Fig. 3 for the three layers nearest to the (100) face of an fcc crystal. The range of in-plane order is similar to the range of layering, and is also related to the pair correlation function.

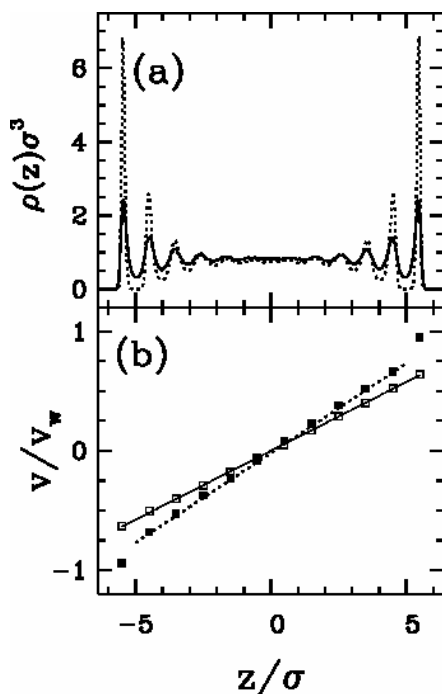


Figure 2. (a) Density as a function of distance between two walls for $\epsilon_w/\epsilon = 0.4$ (solid line) and 4 (dotted line). The wall atoms are centered on the left and right boundaries of the plots. Increasing the attraction to the wall increases the magnitude of the density oscillations, but not the decay length. (b) Velocity divided by the wall velocity v_w as a function of distance between walls for $\epsilon_w/\epsilon = 0.4$ (open squares) and 4 (closed squares). This data is from the low wall velocity regime where the curve is independent of v_w . Points show the average velocity in each layer, and linear fits to each set of points are shown. Note that the velocity extrapolates to a value less than v_w , indicating slip.

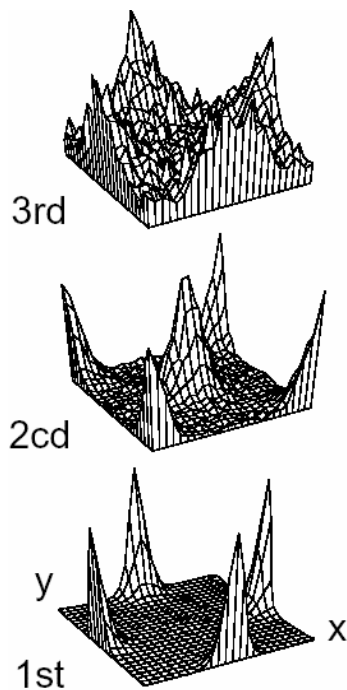


Figure 3. Probability of finding a fluid atom at a given lateral position in the 1st through third layers above a (100) surface of an fcc solid. Only one periodic unit cell of the surface is shown. Wall atoms lie at the center and corners of the cell. Atoms in the first layer lie centered between these wall atoms on the edges of the unit cell. Atoms in the second layer are centered between those on the first layer and so on. (Reproduced from Ref. 32.)

Layering and in-plane order are present near any solid/fluid interface. When the fluid film is thicker than the range of structural change, its main effect is to alter the flow boundary condition. However, when the order spans the entire thickness, the film may begin to exhibit solid-like behavior.

For the spherical molecules of Figs. 2 and 3 the order must be surprisingly large before solidification occurs. This can be seen from Fig. 2(b) where any change in viscosity would produce a change in the velocity gradient (since the stress is constant). All but the last solid square near each wall fall onto a single straight line, implying that the viscosity retains its bulk value down to the first layer. This is true even though the density changes by up to a factor of seven near the second and third layers.⁴⁸ Studies of chain molecules show much smaller density modulations before solidification occurs.

3.4.2 Glass transition

Figure 4 shows how the viscosity changes in the limit of extreme confinement. The spacing between the walls was decreased by (a) decreasing the number of layers at fixed pressure, or (b) increasing pressure at a fixed number of layers. To compare to experiments, an effective shear rate $\dot{\gamma}_{\text{eff}}$ was defined as the velocity difference between two parallel walls divided by their separation. The effective viscosity μ_{eff} is then the shear stress divided by $\dot{\gamma}_{\text{eff}}$.

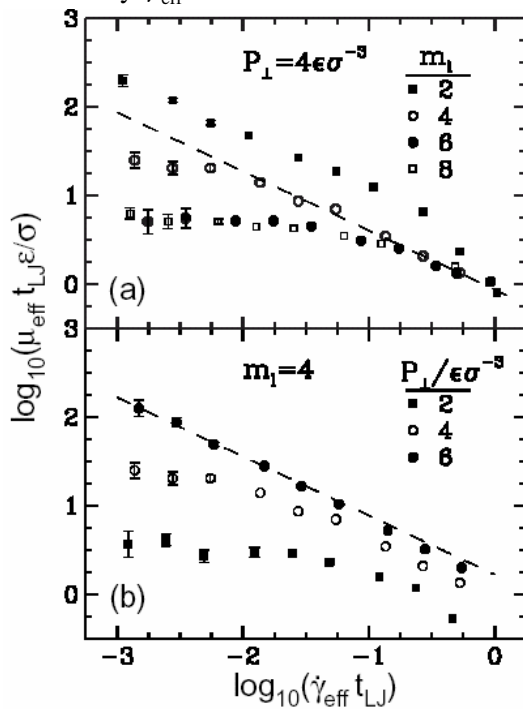


Figure 4. Plots of the effective viscosity μ_{eff} vs. effective shear rate $\dot{\gamma}_{\text{eff}}$ at (a) fixed normal pressure $P_{\perp} = 4\epsilon\sigma^{-3}$ and varying numbers of layers m_l , and (b) fixed $m_l = 4$ and varying P_{\perp} . Dashed lines have slope $-2/3$. (Reproduced from Ref. 14.)

For thick films and low pressures, the viscosity shows a broad Newtonian region where μ_{eff} is constant. The shear rate where the viscosity begins to drop is the inverse of the characteristic relaxation time of the film. As the degree of confinement increases, both the low shear rate viscosity and the relaxation time rise dramatically. These changes are typical of a fluid approaching a glass transition.

Demirel and Granick² showed that the frequency-dependent complex elastic moduli measured at different film thicknesses could be collapsed onto a single universal curve using a generalization of the time-temperature scaling that describes bulk glasses.^{49,50} Baljon and Robbins examined the relationship to bulk glass transitions in more detail.^{15,51} The shear-rate dependent viscosity was calculated for films thick enough to exhibit bulk behavior and the temperature was varied through the glass transition.⁵² Fig. 5 shows that these results can be collapsed onto a universal curve using time-temperature scaling.^{15,51} More importantly, viscosity curves for thin films that were brought through a glass transition by either increasing pressure at fixed number of fluid layers or by decreasing the number of layers at fixed pressure could be collapsed onto the same universal curve. This indicates that the same glass transition occurs whether thickness, normal pressure, or temperature is varied. The effect of walls is similar to that of a change in thermodynamic variables.

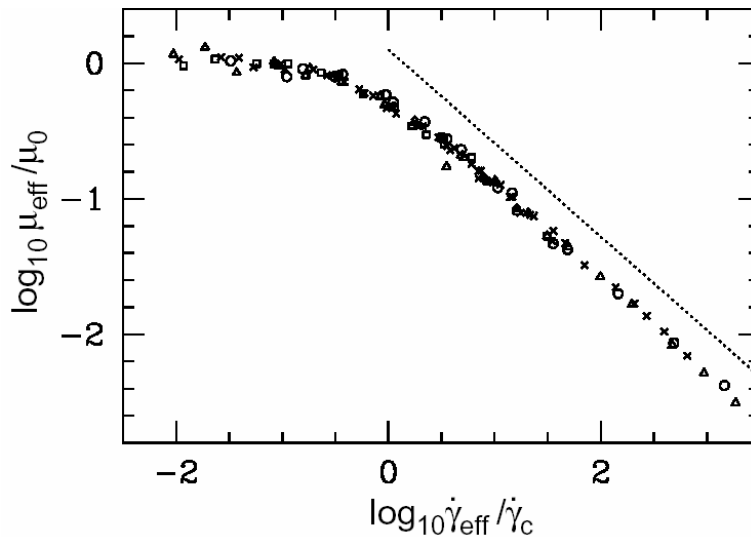


Figure 5. Universal response function for bulk and confined films obtained by scaling the effective viscosity and shear rate. Circles show results for decreasing temperature in bulk systems, squares are results from Fig. 4(a), crosses are from similar runs with different wall interactions, and triangles are results from Fig. 4(b). (Reproduced from Ref. 15.)

4 MOLECULAR ORIGINS OF FRICTION

4.1 How Do Solids Lock Together?

One of the outstanding puzzles in studies of friction has been why macroscopic bodies normally exhibit static friction.⁴¹ That is, they do not move relative to each other until a finite threshold force F_s , or static friction, is exceeded. This implies that the two bodies have locked together into a local energy minimum, and F_s is the force needed to break them free from this minimum.

The first difficulty is to understand how almost any pair of macroscopic bodies manages to lock together.^{10,41,51} Analytic⁵³ and numerical work^{12,16,18,54,55} shows that two crystals should almost always slide over each other without static friction. Static friction only occurs if the alignment and lattice constants are exactly tuned to produce a common periodicity (commensurability), or if the interactions between the two surfaces are strong compared to the interactions within each surface. Surfaces are extremely unlikely to be commensurate, and the interactions between incommensurate surfaces are unlikely to be strong enough to produce locking. Indeed, even calculations for two clean incommensurate surfaces of the same metal show no static friction.^{16,55} One might expect that roughness or other disorder on the surface produces locking, as in charge-density waves and other systems. However scaling analysis shows that the pinning force between three dimensional objects is exponentially weak.⁵⁶⁻⁵⁸

Smith and Robbins⁴¹ noted that most surfaces are coated with a layer of hydrocarbon molecules and other debris that settles out from the air and suggested that glassy behavior of these thin layers might be responsible for static friction. Müser and Robbins considered commensurate, incommensurate and atomically flat amorphous surfaces, that were either bare or had a layer of molecules separating them.¹⁸⁻¹⁹ Bare rigid surfaces only exhibited static friction in the thermodynamic limit if they were commensurate. Adding elasticity only produced locking between bare incommensurate surfaces when the interaction between surfaces was an order of magnitude larger than the internal interactions. In contrast, all surfaces pinned together readily when a monolayer or submonolayer of molecules was placed in between them. Indeed, static friction was observed between rigid commensurate and incommensurate surfaces even when the molecules separating them formed a freely diffusing fluid layer.¹⁸

4.2 Molecular origins of Amontons' laws

The above results indicate that the airborne molecules present between any ambient surfaces can naturally lead to widespread observation of static

friction. The next question is whether the resulting friction is consistent with experiment. Recent work by He *et al.*¹⁷ shows that glassy adsorbed layers provide a simple molecular explanation for Amontons' 300-year-old laws for friction. These state that friction is proportional to the normal load L and independent of the apparent geometric area of the surfaces A_{app} .

He *et al.* built on a phenomenological model developed by Bowden and Tabor.⁶⁰ These authors noted that A_{app} is usually much larger than the area of intimate molecular contact A_{real} . They pointed out that both Amontons' laws and many exceptions to them could be explained *if* the local shear stress, τ , in the contacts increased linearly with the local pressure:

$$\tau = \tau_0 + \alpha P. \quad (3)$$

Summing over A_{real} and dividing by load gives a friction coefficient

$$\mu \equiv F/L = \alpha + \tau_0/P. \quad (4)$$

This is independent of load if P is constant or $\tau_0/P \ll \alpha$. At high loads, both elastic^{58,61} and plastic⁶⁰ models of multiple contacts yield a constant P . At low loads, P decreases, explaining why many systems show an increase in μ in this limit.^{60,62}

Molecular dynamics simulations with commensurate, incommensurate and disordered walls show that adsorbed molecular layers naturally lead to a linear relation between τ and P like that assumed by Bowden and Tabor.^{17,59} This linear relation extends into the gigapascal range that is typical of real contacts. Moreover, τ_s is insensitive to parameters that are not controlled in experiments, including the relative crystallographic orientation of the surfaces, sliding direction, chain length, chain density, *etc.* These results can be understood from simple geometric arguments¹⁷ and a microscopic theory.⁵⁹

Figure 6 illustrates some of the walls that were studied. In each case the bottom wall is a (111) surface of an fcc crystal with nearest neighbor spacing $d=1.2\sigma$. In (A-C) the top wall is identical, but is rotated by 0, 8.2 or 90°, respectively. In (D), the lattice constant of the top wall is slightly smaller than that of the bottom wall. Only (A) is commensurate.

4.2.1 Results for Static Friction

The static shear stress τ_s for each system and pressure was determined by increasing the force until the system began to slide steadily. The static friction was zero when no atoms were placed between the surfaces, except for the commensurate case (Fig. 6(A)).

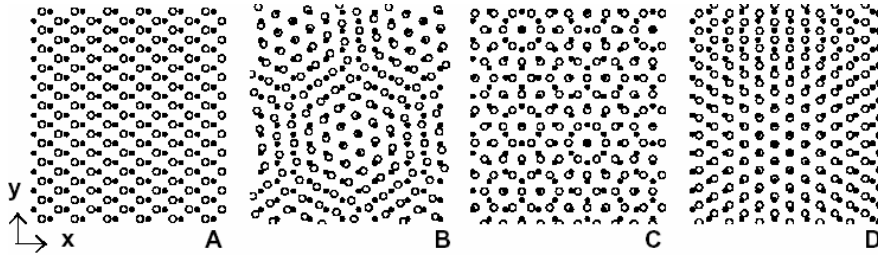


Figure 6. Projections of atoms from the bottom (filled circles) and top (open circles) surfaces into the plane of the walls. In A-C the two walls have the same structure and lattice constant but the top wall has been rotated by 0°, 8.2° or 90°, respectively. In D the walls are aligned, but the lattice constant of the top wall has been reduced by 12/13. Note that the atoms can only achieve perfect registry in the commensurate case A. The simulation cell was at least four times the area shown here. (Reproduced from Ref. 17.)

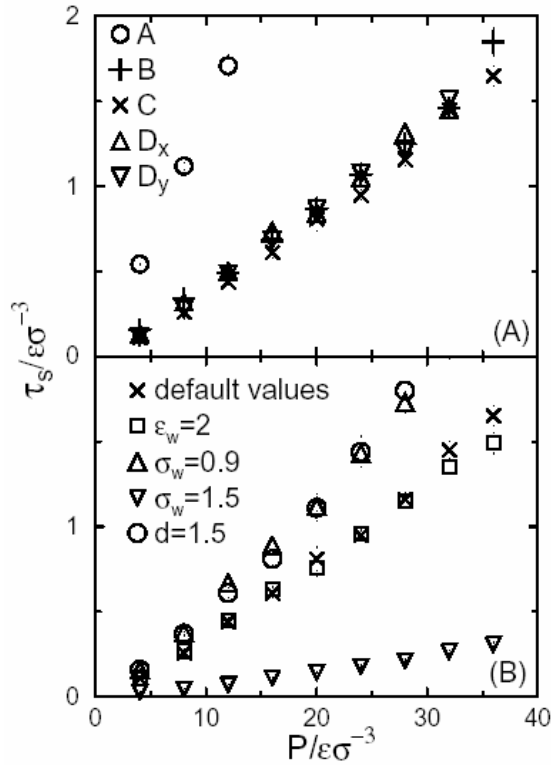


Figure 7. Variation of the yield stress τ_s with pressure P for (a) coverage equal to 1/8 for the different walls shown in Fig. 6. The results for incommensurate surfaces are independent of sliding direction as illustrated for sliding along x (up triangles) and y (down triangles). Panel (b) shows results for different potential parameters. The default values are $n = 6$, $\epsilon_w = \epsilon$, $\sigma_w = \sigma$, $d = 1.2\sigma$, $r_c = 2^{1/6}\sigma$, and $k_B T = 0.7\epsilon$. (Reproduced from Ref. 17.)

Fig. 7(a) compares τ_s for the different surfaces shown in Fig. 6 at an adsorbate coverage of 1/8, defined as the ratio of monomers to wall atoms on each surface before they are brought into contact. For each case the data

fall onto the straight line implied by Equation 3 up to $P=36\varepsilon/\sigma^3$ or about 1.5 GPa. The incommensurate cases [Fig. 6(B)-(D)] all give very similar values of τ . Changing the direction of sliding also has little effect on τ , as indicated by the comparison between sliding along x or y for the surfaces of Fig. 6(D) [up and down triangles in Fig. 7(a)]. Only the commensurate case [Fig. 6(A)] produces different values of τ_s . As expected, the friction is enhanced because of the uniform registry between the two surfaces. However, the ratio between commensurate and incommensurate values of α has been reduced from infinity to a factor of three due to the presence of an adsorbed layer.

A variety of interaction potentials and geometries have been considered to determine which factors influence α and τ_0 and which leave them unchanged. The alignment of the surfaces and the direction of sliding always leave τ_s nearly unchanged, except in the unlikely case where the surfaces are commensurate. Other parameters that are not controlled in experiments have little effect on the friction. For example, decreasing the chain length n from 6 to 3 to 1 produces no change in τ_s , within statistical fluctuations. Increasing the coverage on each surface up to one or more monolayers on separated surfaces also produces little change in τ_s .

Since different materials do have different experimental friction coefficients, some potential parameters must change τ_s . Fig. 7(b) shows the effect of changing one parameter at a time from our standard set. Increasing $\varepsilon_w/\varepsilon$ from one to two produces almost no change in τ_s . In contrast, decreasing σ_w/σ from 1 to 0.9 increases α by 50% and increasing this ratio to 1.5 decreases α by a factor of 6. The opposite trend is seen for d/σ , where an increase from 1.2 to 1.5 increases α to 0.073.

These trends can be understood from a simple geometric argument. At the large pressures of interest, the repulsive interactions between wall atoms and monomers are dominant. Atoms and monomers cannot be closer than an effective hard sphere diameter of order σ_w . This is very insensitive to pressure because the repulsive force rises as $(\sigma_w/r)^{-13}$ as r decreases. For the same reason, changing σ_w by a factor of two has little effect on the system. In contrast, decreasing σ_w/d allows monomers to penetrate more deeply into the wells between wall atoms. Tracing out the height of closest approach as a function of lateral displacement produces a ramped surface. The value of α corresponds to the effective slope of the ramps, as envisioned in the early models of friction.⁶³ As σ_w/d decreases, the ramp becomes steeper, resulting in the increase in α seen in Fig. 7(b). We have confirmed that the surfaces do indeed move apart as the yield stress is approached and that this displacement increases with α .

4.2.2 Kinetic Friction

In recent studies we have examined the influence of adsorbed layers on kinetic friction.⁶⁴ We find that the friction rises logarithmically with sliding velocity v as observed in many experiments.⁶⁵ As for static friction, $\tau(v)$ rises linearly with P over the experimentally relevant range of pressures. Moreover the kinetic and static friction follow the same trends with ε_w , σ_w and other parameters. At the lowest velocities accessible to our simulations \sim cm/s, the kinetic friction is usually 70 to 90% of the static friction. Such ratios are typical of many experiments with dry surfaces.

5 CONCLUSIONS

The field of nanotechnology offers great opportunities for fundamental science as well as industrial impact. Experimental systems continue to become better characterized and smaller in scale, while simulations increase in scale and complexity. There is already considerable overlap between the two, and promise for closer interplay between them in the future.

The work presented here emphasizes the important role that surface species can play. Two general factors that have yet to be addressed in detailed simulations are surface roughness and long-range elastic deformations. These effects and detailed models of molecular structure and bonding will be needed to improve comparisons of theory and experiment.

ACKNOWLEDGMENTS

The authors wish to thank Drs. A. R. C. Baljon, M. Cieplak, G. S. Grest, M. H. Müser, P. M. McGuiggan and P. A. Thompson for useful discussions. Support from the National Science Foundation Grant DMR-9634131 is gratefully acknowledged.

REFERENCES

- 1 M. L. Gee, P. M. McGuiggan, J. N. Israelachvili, and A. M. Homola, *J. Chem. Phys.* **93**, 1895 (1990).
- 2 A. L. Demirel and S. Granick, *Phys. Rev. Lett.* **77**, 2261 (1996).
- 3 H.-W. Hu, G. A. Carson, and S. Granick, *Phys. Rev. Lett.* **66**, 2758 (1991).
- 4 J. Krim, E. T. Watts, and J. Digel, *J. Vac. Sci. Technol. A* **8**, 3417 (1990); J. Krim, D. H. Solina, and R. Chiarello, *Phys. Rev. Lett.* **66**, 181 (1991).
- 5 C. M. Mate, G. M. McClelland, R. Erlandsson, and S. Chiang, *Phys. Rev. Lett.* **59**, 1942 (1987).
- 6 R. W. Carpick and M. Salmeron, *Chem. Rev.* **97**, 1163 (1997).
- 7 P. Berthoud and T. Baumberger, *Proc. R. Soc. Lond A* **454**, 1615 (1998).

- 8 A. J. Gellman, *J. Vac. Sci. Technol. A* 10, 180 (1992); C. F. McFadden and A. J. Gellman, *Surf. Sci.* 391, 287 (1997).
- 9 J. H. Dieterich and B. D. Kilgore, *Tectonophysics* 256, 219 (1996).
- 10 M. O. Robbins and M. H. Müser, in *Modern Tribology Handbook*, edited by B. Bhushan (CRC Press, Boca Raton, 2001) pp. 717-765 and cond-mat/0001056.
- 11 J. A. Harrison, S. J. Stuart, and D. W. Brenner, in *Handbook of Micro/Nanotribology*, edited by B. Bhushan (CRC Press, Boca Raton, 1999), pp. 525-594.
- 12 M. Cieplak, E. D. Smith, and M. O. Robbins, *Science* 265, 1209 (1994); E. D. Smith, M. Cieplak, and M. O. Robbins, *Phys. Rev. B.* 54, 8252 (1996).
- 13 J. Klein and E. Kumacheva, *Science* 269, 816 (1995).
- 14 P. A. Thompson, G. S. Grest, and M. O. Robbins, *Phys. Rev. Lett.* 68, 3448 (1992); P. A. Thompson, M. O. Robbins, and G. S. Grest, *Israel J. of Chem.* 35, 93 (1995).
- 15 M. O. Robbins and A. R. C. Baljon, in *Microstructure and Microtribology of Polymer Surfaces*, edited by V. V. Tsukruk and K. J. Wahl (American Chemical Society, Washington DC, 2000), pp. 91-117.
- 16 M. Hirano and K. Shinjo, *Phys. Rev. B* 41, 11837 (1990); K. Shinjo and M. Hirano, *Surface Science* 283, 473 (1993).
- 17 G. He, M. H. Müser, and M. O. Robbins, *Science* 284, 1650 (1999), and G. He and M. O. Robbins, *Phys. Rev. B* 64, 035413 (2001).
- 18 M. H. Müser and M. O. Robbins, *Phys. Rev. B* 64, 2335 (2000).
- 19 M. P. Allen and D. J. Tildesley, *Computer Simulation of Liquids* (Clarendon Press, Oxford, 1987).
- 20 K. Kremer and G. S. Grest, *J. Chem. Phys.* 92, 5057 (1990).
- 21 W. Tschöp, K. Kremer, J. Batoulis, T. Bürger, and O. Hahn, *Acta Polym.* 49, 61 (1998); 75 (1998).
- 22 M. J. Stevens and M. O. Robbins, *Phys. Rev. E* 48, 3778 (1993).
- 23 E. Manias, G. Hadziioannou, and G. T. Brinke, *J. Chem. Phys.* 101, 1721 (1994).
- 24 R. Khare, J. J. de Pablo, and A. Yethiraj, *Macromolecules* 29, 7910 (1996).
- 25 U. Landman, W. D. Luedtke, and J. Gao, *Langmuir* 12, 4514 (1996).
- 26 E. D. Reedy, Jr., *Engineering Fracture Mech.* 36, 575 (1990).
- 27 O. Vafek and M. O. Robbins, *Phys. Rev. B* 60, 12002 (1999).
- 28 J. A. Hurtado and K. S. Kim, *Proc. R. Soc. Ser. A. (London)* 455, 3363 (1999).
- 29 P. A. Thompson, W. B. Brinckerhoff, and M. O. Robbins, *J. Adhesion Sci. Technol.* 7, 535 (1993).
- 30 P. A. Thompson and M. O. Robbins, *Phys. Rev. Lett.* 63, 766 (1989).
- 31 D. Y. C. Chan and R. G. Horn, *J. Chem. Phys.* 83, 5311 (1985); J. N. Israelachvili, *J. Colloid Interface Sci.* 110, 263 (1986).
- 32 P. A. Thompson and M. O. Robbins, *Phys. Rev. A* 41, 6830 (1990).
- 33 P. A. Thompson and S. M. Troian, *Nature* 389, 360 (1997).
- 34 J.-L. Barrat and L. Bocquet, *Phys. Rev. Lett.* 82, 4671 (1999).
- 35 P. G. de Gennes, *C. R. Acad. Sci. Ser. B* 288, 219 (1979).
- 36 J. M. Georges, S. Millot, J. L. Loubet, A. Touck and D. Mazuyer, in *Thin Films in Tribology*, edited by D. Dowson, C. M. Taylor, T. H. C. Childs, M. Godet, and G. Dalmaz (Elsevier, Amsterdam, 1993), pp. 443-452.
- 37 J. N. Israelachvili, P. M. McGuiggan, and A. M. Homola, *Science* 240, 189 (1988).
- 38 E. Manias, I. Bitsanis, G. Hadziioannou, and G. T. Brinke, *Europhys. Lett.* 33, 371 (1996).
- 39 J. Gao, W. D. Luedtke, and U. Landman, *Phys. Rev. Lett.* 79, 705 (1997); *J. Chem. Phys.* 106, 4309 (1997); *J. Phys. Chem. B* 101, 4013 (1997).
- 40 I. Bitsanis, S. A. Somers, H. T. Davis, and M. Tirrell, *J. Chem. Phys.* 93, 3427 (1990); I. Bitsanis and C. Pan, *J. Chem. Phys.* 99, 5520 (1993).
- 41 M. O. Robbins and E. D. Smith, *Langmuir* 12, 4543 (1996).
- 42 F. F. Abraham, *J. Chem. Phys.* 68, 3713 (1978).
- 43 S. Toxvaerd, *J. Chem. Phys.* 74, 1998 (1981).

- 44 I. K. Snook and W. van Meegen, *J. Chem. Phys.* 72, 2907 (1980).
- 45 P. A. Thompson and M. O. Robbins, *Science* 250, 792 (1990).
- 46 U. Landman, W. D. Luedtke, and M. W. Ribarsky, *J. Vac. Sci. Technol. A* 7, 2829 (1989).
- 47 M. Schoen, C. L. Rhykerd, D. J. Diestler, and J. H. Cushman, *J. Chem. Phys.* 87, 5464 (1987); *Science* 245, 1223 (1989); M. Schoen, J. H. Cushman, D. J. Diestler, and C. L. Rhykerd, *J. Chem. Phys.* 88, 1394 (1988).
- 48 Note that if one defines the velocity gradient on a finer mesh, there are fluctuations in slope. The concept of a bulk viscosity is meaningless at such small scales.
- 49 J. D. Ferry, *Viscoelastic Properties of Polymers*, 3rd Ed. (Wiley, New York, 1980).
- 50 W. Götze and L. Sjögren, *Rep. Prog. Phys.* 55, 241 (1992).
- 51 M. O. Robbins, in *Jamming and Rheology: Constrained dynamics on microscopic and macroscopic scales*, edited by A. J. Liu and S. R. Nagel (Taylor and Francis, London, 2000) and cond-mat/9912337.
- 52 A. R. C. Baljon and M. O. Robbins, *Mat. Res. Soc. Bull.* 22(1), 22 (1997); and in *Micro/Nanotribology and Its Applications*, edited by B. Bhushan (Kluwer, Dordrecht, 1997), pp. 533–553.
- 53 S. Aubry, in *Solitons and Condensed Matter Physics*, edited by A. R. Bishop and T. Schneider (Springer-Verlag, Berlin, 1979), pp. 264–290. P. Bak, *Rep. Prog. Phys.* 45, 587 (1982).
- 54 B. N. J. Persson, *Phys. Rev. B* 48, 18140 (1993).
- 55 M. R. Sørensen, K. W. Jacobsen, and P. Stoltze, *Phys. Rev. B* 53, 2101 (1996).
- 56 B. N. J. Persson and E. Tosatti, in *Physics of Sliding Friction*, edited by B. N. J. Persson and E. Tosatti (Kluwer, Dordrecht, 1996), pp. 179–189.
- 57 C. Caroli and P. Nozieres, in *Physics of Sliding Friction*, edited by B. N. J. Persson and E. Tosatti (Kluwer, Dordrecht, 1996), pp. 27–49.
- 58 A. Volmer and T. Natterman, *Z. Phys. B* 104, 363 (1997).
- 59 M. H. Müser, L. Wenning, and M. O. Robbins, *Phys. Rev. Lett.* 86, 1295 (2001) and cond-mat/0004494.
- 60 F. P. Bowden and D. Tabor, *The Friction and Lubrication of Solids* (Clarendon Press, Oxford, 1986).
- 61 J. A. Greenwood and J. B. P. Williamson, *Proc. Roy. Soc. A* 295, 300 (1966).
- 62 E. Rabinowicz, *Friction and Wear of Materials* (Wiley, New York, 1965).
- 63 D. Dowson, *History of Tribology* (Longman Inc., New York, 1979).
- 64 G. He and M. O. Robbins, *Tribol. Lett.* 10, 7 (2001) and cond-mat/0008196.
- 65 J. H. Dieterich, *J. Geophys. Res.* 84, 2169 (1979).